Grain Boundary Chemistry of Alloy 718-Type Alloys

R. G. Thompson, M. C. Koopman, and B. H. King

The University of Alabama at Birmingham

Abstract

Grain boundary chemistries of 718-type alloys doped with B, P, S, and/or C were studied to determine the segregation behavior of these elements. Specimens were intergranularly embrittled by hydrogen charging. These embrittled specimens were fractured in the ultra-high vacuum of a scanning Auger microprobe. Surface chemistries and depth profiles of these freshly fractured specimens were taken. Typical features analyses were grain boundary surfaces, fractured matrix surfaces, carbide-matrix interfaces, Laves-matrix interfaces, cleaved carbide surfaces, and sulfide-matrix interfaces. It was found that B segregated uniformly to grain boundary surfaces as did P and S when these elements were present as intentional additives. Sulfur segregated to carbide and Laves phases interfaces even when the sulfur level was kept as low as possible. No strong evidence of competition between these elements for grain boundary segregation was found. Implications of these results relative to element partitioning during solidification, constitutional liquation of carbides and the mechanism of intergranular liquation cracking.

Introduction

The bulk chemistry of 718-type alloys is formulated to serve various purposes such as: ease of processing, high temperature solid solution strength, γ' and γ'' precipitation for age hardening, and carbides for grain size control. Apart from the bulk chemistry, the chemistry of the grain boundaries is considered important to prevent stress rupture and B and Zr are added to strengthen the boundaries. While the structure-property relationships for the bulk alloy have been studied extensively, similar studies on the grain boundary and precipitate interfaces have not been published. This paper presents the results of a study on the effects of minor alloying and impurity elements, and processing on the interfacial chemistry of alloy 718.

The effects of certain non-metallic impurities (S and P) and the minor alloying additions (C and B) on the mechanical properties of superalloys are well documented; however, these elements are also suspected of significant intergranular effects yet

Superalloys 718, 625 and Various Derivatives
Edited by Edward A. Loria
The Minerals, Metals & Materials Society, 1991

information on the actual interfacial chemistries involved is limited.(1,2,3) The development of Auger electron spectroscopy (AES) techniques allows for compositional analysis of the top few atomic layers of a solid surface. This makes it possible to determine, experimentally, interfacial chemistries when measurable interfacial surface areas can be exposed by means of freshly fracturing samples in a ultra-high vacuum environment. Because of the metallurgical design of the nickel superalloys, intergranular fracture areas are difficult to obtain without altering the interfacial chemistry of the material. Previous AES studies of superalloys have utilized either hot stages or high temperature tensile devices which are known to cause interfacial segregation. With hydrogen embrittlement of 718, caused by large concentrations of interstitially absorbed or adsorbed hydrogen, a reversible method is available to produce fracture separation at grain boundary surfaces and γ-matrix/second phase interfaces without altering the segregation behavior of the elements found there.(4)

Much has been published on detrimental effects of sulfur segregation to grain boundaries in high nickel superalloys and its prevention by the addition of gettering elements (Ti, Zr, Hf, La, and Mg) which form primary sulfides.(3,5) Early work by Merica and Waltenberg attributed sulfur's effects to the formation of a Ni-Ni_3S_2 eutectic film but more recent studies suggest that a low melting grain boundary phase is not necessary for high temperature intergranular failure.(6) Less information has been reported on the embrittling of superalloy grain boundaries by phosphorus, however, the information available supports the hypothesis that phosphorus segregates to grain boundaries. It has also been reported that impurity enriched grain boundaries decrease intergranular embrittlement by hydrogen.(7,8,9)

Both carbon and boron are intentional minor additions to 718. Residual carbon in the form of MC carbides have been identified cellularly and intragranularly in many commercial nickel-iron base superalloys including 718. Because carbon is used as a refining agent to deoxidize and desulfurize the charge and at the same time influences the fluidity and castability of liquid metal, carbon levels must be carefully controlled.

Boron in the range of 0.003-0.030% is standardly added to improve stress rupture properties and hot workability of these alloys.(10) Direct evidence for the atomic segregation of boron at some grain boundaries and for boride precipitation at others has been reported.(11) The beneficial effects of boron are believed to be due to its ability to reduce grain boundary diffusion reactions and so delay the formation of denuded zones.

Given the various and important relationships between impurity and minor alloy additions and intergranular material properties, it is important to understand the interactions of these elements

at both grain boundaries and precipitate interfaces. This study is the first to examine these interfacial chemistries in alloy 718 as a function of alloy composition and processing.

Experimental Procedure

The experimental procedure consisted of preparing compositions of 718-type alloy for fracture and surface analysis in a scanning Auger microprobe.

Compositions

The 718-type compositions were developed along two routes because they were used in other studies. The first route (A) consisted of four alloys, two developed from a low carbon heat (20A,22A) and two from a high carbon heat (25A,27A). These two heats were modified to give a high and low sulfur heat for each carbon level (Table I). These alloys were examined in the as-cast and heated treated conditions (Table II). The second route (B) was one in which seven heats were developed from controlled additions of many elements. The elemental additions and deletions were based on either the principle of using the maximum or minimum limit of the specification or an element was made as low as possible which was at least less than 10 ppm. This was used to make controlled additions of boron, sulfur, carbon, and phosphorus. These alloys were cast, mechanically worked, and recrystallized (Table II).

Table I Carbon, Sulfur, Phosphorus and Boron Levels for the Different Heats of Alloy 718*

		C	S	P	B	Nb	Si
Heat							
3B	BSP	<.001	.015	.015	.01	5.4	<.001
5B	PSCP	.1	.015	.015	.01	4.4	.35
10B		.1	0.015	<.001	<.001	4.4	<.001
11B	SC	.1	<.001	<.001	<.001	4.4	<.001
12B	BC	.1	<.001	<.001	.01	4.4	<.001
13B	B	<.001	<.001	<.001	.01	5.4	<.001
14B	P	<.001	.015	.015	<.001	5.4	<.001
20B	-	<.001	<.001	<.001	<.001	4.4	<.001
20A**	-	.021	<.001	.001	.002	4.4	.01
22A	S	.021	.009	.001	.003	5.1	.01
25A	C	.060	<.001	.001	.002	4.4	.01
27A	CS	.060	.009	.001	.003	5.1	.01

* The remainder of the chemical composition is within normal ASM-5383 specifications for Alloy 718.

** A - As-cast material and
B - thermomechanically treated to recrystallize as-cast material.

Table II Specimen Processing

Group A {Heats 20A, 22A, 25A, 27A}
As-Cast, Grain Size Approximately 100 μm

Group A {Heat 27A}

Homogenization:	1 hour at 1093°C
Solution Anneal:	1 hour at 927°C
Step Cool:	1 hour at 1093°C
	1 hour at 927°C
	10 hours at 760°C
	10 hours at 649°C

Group B {Heats 3B, 5B, 11B, 12B, 13B, 14B, 20B}
Step 1: 20% Cold Rolled, 30 minutes at 1000°C
Step 2: 15% Cold Rolled, 60 minutes at 1000°C
60 minutes at 1100°C

(Equiaxed Grain Size 20 - 50 μm)

Scanning Auger Microprobe

Samples for Auger analysis were cut to approximate dimensions of 1mm x 1mm x 10mm, notched, and electrolytically charged to promote hydrogen embrittlement of the grain boundaries. The process of hydrogen charging involved spot welding the sample to a platinum wire, and suspending within a platinum basket in an ambient temperature electrolyte composed of .5 M Sulfuric acid with 50mg of $NaAsO_2$/L (added as a catalytic poison to encourage hydrogen absorption). A constant current density of 400 ma/cm2 was applied to the cell and the solution was mechanically stirred. The samples were exposed to hydrogen charging from 13 to 25 days. The samples were cleaned in successive baths of: dilute HC1, distilled water, and ethanol. After immediately loading into the UH vacuum of the Auger microprobe, the samples were fractured in situ by applying a slow strain rate at the notch. A 10 KV electron beam with a 1 to 2 micron diameter was used to gather dN(E)/dE Auger spectra of exposed grain boundaries, second phase precipitates and cleaved matrix areas. After acquiring spectra from areas of interest on the fracture surface, selected areas were ion sputtered with argon and subsequent spectra collected for comparison.

Results

Microstructure

The microstructures of specimen in this study were seen to vary with composition and processing. The carbide to Laves phase ratio varied primarily with the C/Nb ratio in all heats. This varied somewhat with the magnitude of minor alloy and impurity additions in group B alloys. The recrystallized alloys developed a grain size of about 20-40 microns with a range of second phase faction from about 0% for alloy 20B (Figure 1) to 2% in alloy 13B (Figure 2). The cast alloys had a dendritic structure (Figure 3). Heat treatment typically reduced the volume fractions of both carbide and Laves phase by as much as half.

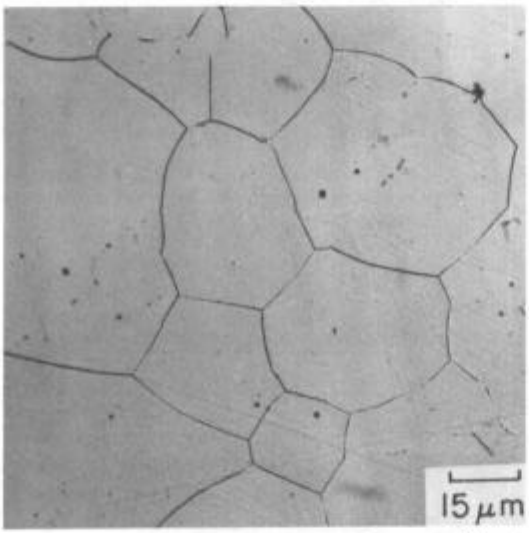

Figure 1 - Typical microstructures of recrystallized Alloy 20B having low levels of carbon, niobium, sulfur, phosphorus and boron.

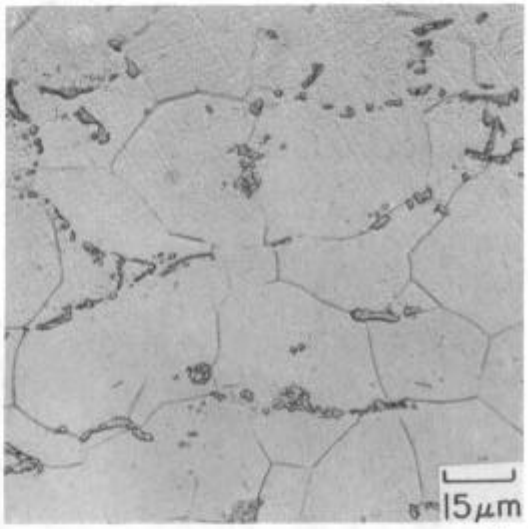

Figure 2 - Typical microstructure of recrystallized Alloy 13B having high boron and niobium levels.

Fracture Surfaces

Extensive cathodic charging of these alloys with hydrogen produced fracture surfaces that included matrix cleavage, carbide cleavage, microvoid coalescence, grain boundary, carbide-matrix interface, eutectic interfaces, and sulfides. Figure 4 shows fracture along multiple grain boundaries, typical of recrystallized Group B alloys, usually found within 0.2mm of the outside perimeter of the fracture surface. Figure 5 shows isolated grain boundary fracture, characteristic of as-cast Group A alloys. As-cast alloys usually exposed only one face of a grain boundary during fracture, this being surrounded by transgranular cleavage planes and carbides. Carbides and laves

phase were seen to fracture in a brittle fashion. Eutectic areas, as seen in Figure 6, fractured exposing a mixture of Laves and carbides.

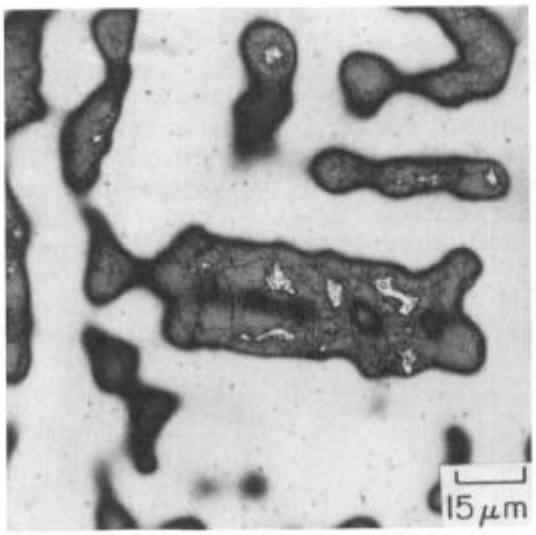

Figure 3 - Microstructure of as-cast specimen of heat 25A having a high sulfur level. 500X.

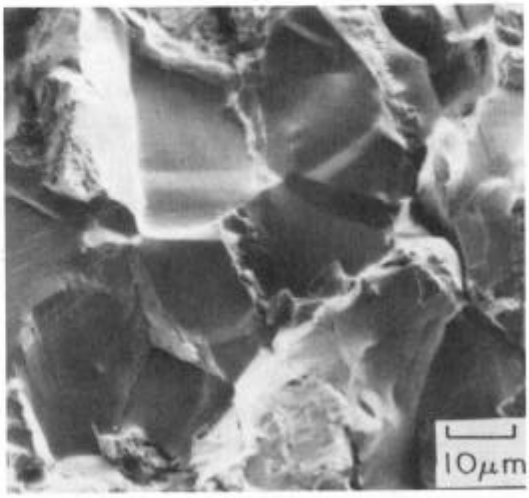

Figure 4 - Typical freshly fractured grain boundary surfaces as seen in the small grain sized recrystallized Alloy 718.

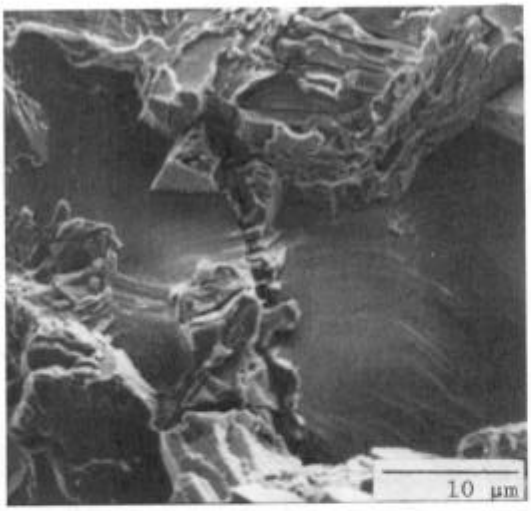

Figure 5 - Typical freshly fractured grain boundary surface as seen in large grain as-cast Alloy 718.

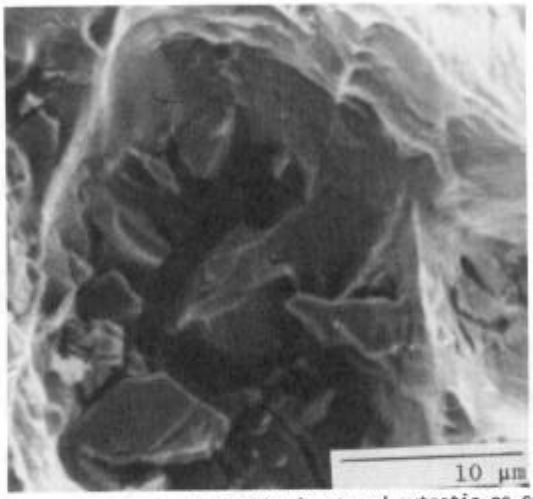

Figure 6 - Typical freshly fractured eutectic as seen in Alloy 718.

Auger Analysis

Exposed surfaces were analyzed by Auger Electron spectroscopy. The grain boundaries showed segregation of boron, phosphorous and sulfur at grain boundaries in varying concentrations depending on their concentration in the alloy. In addition, sulfur was often seen to be segregated to the carbide-matrix and laves-matrix interfaces, while boron and phosphorous were not. Figure 7, a typical Auger spectrum collected from a grain boundary, shows the presence of both phosphorus and sulfur. A typical carbide-matrix interface spectrum is shown in Figure 8. This spectra exhibits a characteristic signature of carbon, titanium, nitrogen and niobium, in addition to a layer of segregated sulfur. Sulfur was also seen to segregate strongly to the laves-matrix interface, Figure 9. Spectra were collected from various exposed surfaces after ion sputtering and from cleavage planes of the matrix for comparison with grain boundaries. The matrix spectra and sputtered surfaces were typically devoid of S, P and B (Figure 10).

Intensity values of examined elements were gathered by measuring peak-to-valley amplitudes of dN/dE spectra, and ratioed to that of nickel for reference. Measured intensities for all alloys are given in Appendix A.

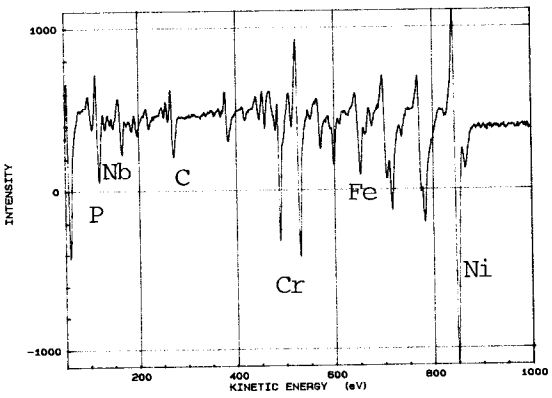

Figure 7 - Scanning Auger Microprobe (SAM) chemical spectra of in situ grain boundary surface.

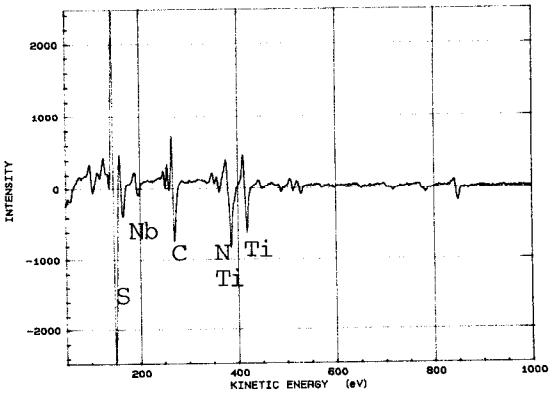

Figure 8 - Typical SAM chemical spectra of freshly fractured carbide surface.

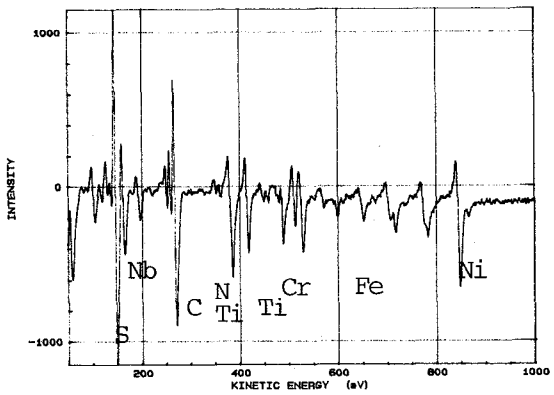

Figure 9 - Typical SAM chemical spectra of freshly fractured eutectic surface.

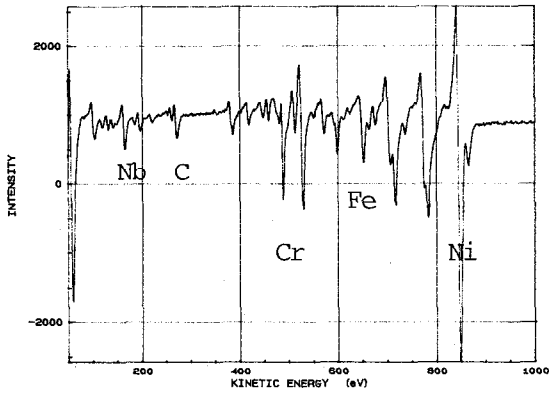

Figure 10 - Typical SAM chemical spectra of freshly fractured matrix surface.

Discussion

A good deal of interface segregation data was generated on 718-type alloy compositions during this study. The alloys varied significantly in impurity and alloy composition as well as heat treatment. Considerable thought has gone into organizing and evaluating the data so that trends can be recognized and discussed. The following paragraphs describe how the data was organized and then proceeds to discuss the observed trends.

Reduction of Auger Data

The Auger data presented in Appendix A is not easily digested for analysis. A first order reduction of data has already been performed in Appendix A by normalizing the differential peak-to-peak height with respect to the primary nickel peak. This was done to help eliminate variations in the machine operating characteristics that inevitably occured over the 18 month period during which data was collected (about 700 machine hours).

A second data reduction procedure was used to develop the surface excess data given in Table III. The surface excess was defined as the difference between the normalized intensity of the freshly fractured surface spectra and the surface spectra after ion sputtering the exposed surface to remove a few surface layers of atoms. In some cases where sputtering was not performed, the matrix was used for comparison to the surface as noted in Table III. No attempt is made to present the data in quantitative or semiquantitative form. The surface excesses, however, provide a reasonable format for comparison of relative effects of alloy chemistry, processing, and heat treatment on the distributions of certain elements at the interfaces of 718-type alloys.

Contributions to Interface Spectra

Before proceeding, it is worth noting several caveats of the investigation process. The 718-type alloys produce solidification microstructures which contained some or all of

the following: γ-matrix, MC-type carbides (mainly NbC), sulfides, and eutectic zones with Laves plus the other phases in various proportions. The electron beam diameter used for Auger analysis was in the 0.5 to 2 μm range depending on the spatial resolution necessary for the surface under investigation. The largest spot size possible was always used in order to maximize the Auger signal. Carbides were particularly easy to analyze because a sufficient number of carbides greater than 2 μm were generally available for analysis. Grain boundaries were usually easy to analyze since intergranular precipitates were generally easy to identify and avoid during analysis. However, it is possible that intergranular precipitates smaller than the resolution of the microscope (about 0.1 μm) existed on the exposed surface and contributed to the Auger spectra. The contribution of such small, isolated precipitates to the overall intensity of the spectra would also be small. Sulfides were easy to identify but were generally smaller than the lateral resolution of the electron beam. This meant that surrounding matrix/surface was usually present in spectra from these particles. Finally, the individual constituents of the eutectic zones were sometimes smaller than the lateral resolution of the electron beam. Thus, it could be possible to have contributions from various constituents in the spectra of the eutectic zone. Based on the foregoing discussion, it was decided to rely on information from carbide and grain boundary surfaces for evaluation of the interfacial distribution of elements whenever possible.

Sulfur

Sulfur is well known and well documented for its surface activity in pure and dilute nickel.(3) However, it has been shown that sulfur scavengers can prevent interface segregation in dilute nickel alloys.(12,13) Thus, the behavior of sulfur in nickel superalloys was highly speculative. The results concerning sulfur in this study are quite interesting and some trends are easily explained.

Sulfur Distribution Following Casting

Table III Interfacial Sulfur Levels in Excess of Sputter Cleaned Surfaces for As-Cast Specimens

Alloy Composition		Heat #	Carbide Surface	GB
High C	High S	(#27A)	1.8	0.11
		(#27A)	4.3	0.09
Low C	High S	(#25A)	1.7	0.00
High C	Low S	(#22A)	0	0.02
		(#22A)	0	0.03
Low C	Low S	(#20A)	0	0.02

Sulfur distribution following casting is dependent on the sulfur level present. The high sulfur alloys (0.009) always exposed a carbide-matrix interface with a very high excess in S. The low sulfur heats gave carbide surfaces with no excess sulfur. The fact that no excess sulfur was found indicates that these carbides did not have enough sulfur to cause fracture at the carbide-matrix interface so that the exposed surface is really a cleavage plane through the carbide.

The grain boundary excess sulfur is low relative to the excess at the carbide-matrix interface. Since grain boundary fracture was easy to distinguish from cleavage in the matrix, it is thought these levels of grain boundary sulfur are typical of the heat and its particular cooling rate following casting.

Several interesting aspects of sulfur distribution during solidification of 718-type alloys are evident from these results. The alloys just discussed solidify in the following sequence:

$$L \rightarrow \gamma \rightarrow \gamma+MC \rightarrow \gamma+MC + \text{Eutectic} \qquad (1)$$

This is verified by the differential thermal analysis of the alloys as given in Figure 11. For sulfur to be highly concentrated at the carbide-matrix interface, it must be insoluble in both phases and driven to the liquid phase during solidification. An alternate possibility is that sulfur is soluble at high temperatures in γ-matrix and/or carbide and is rejected to the interface in the solid state during cooling. If this were the case for γ-matrix, sulfur would show a greater excess at the grain boundaries. Thus, it can be concluded that sulfur is rejected by γ-matrix during solidification and accumulates in the liquid phase where it eventually becomes trapped at carbide and eutectic interfaces and/or precipitated as a sulfide. Another possibility is that sulfur is gettered at the carbide interface which also has an excess of N and Ti.

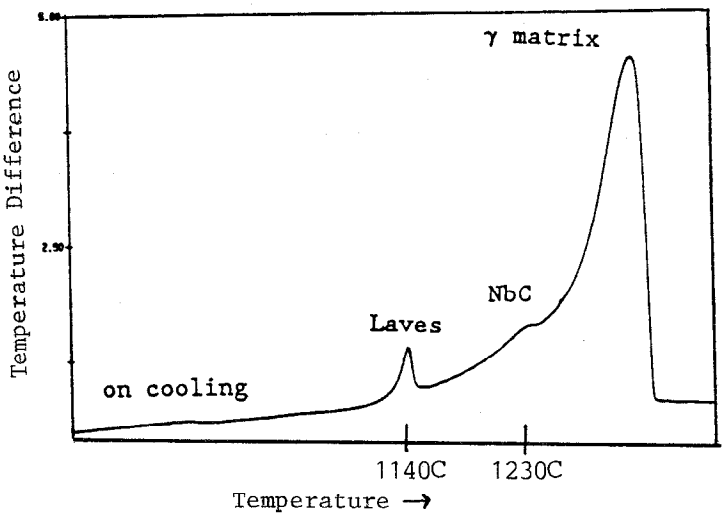

Figure 11 - A differential thermal analysis, DTA, thermogram for the melting and solidification of heat 22 (0.06 wt%C and <0.001 wt%S).

It is interesting to observe that sulfur weakens the carbide-matrix interface. The exact amount of sulfur needed to cause the transition from carbide cleavage to carbide-matrix interface fracture cannot be calculated from Auger data. However, such behavior may signal a cause of low toughness in as-cast hardware or possibly a preferred interaction path for hydrogen and other embrittling mechanisms.

The data for sulfur at the eutectic is less convincing than that for the carbides. Sulfur is present at the exposed eutectic zone but it can not easily be traced to a certain interface in most cases. The data does show that excess sulfur is found on both carbides and laves in this area of the microstructure.

Sulfur Redistribution During Heat Treatment

Table IV Interfacial Sulfur Levels in Excess of Sputter Cleaned Surfaces for As-Cast Plus Heat Treated Specimens

	Heat #	Carbide Surface	GB
AS CAST	(#27A)	4.3	0.11
HOMOGENIZED	(#27A)	1.8	0.03
SOLUTION ANNEAL	(#27A)	1.1	0.00
STEP COOLED	(#27A)	0.1	2.20

The redistribution of sulfur during heat treatment appears to follow the theory of equilibrium segregation of impurities to grain boundaries.(14) At high temperatures such as homogenization or solution annealing, no grain boundary segregation occurs. There may even be a reduction of excess sulfur as these high temperature treatments can reverse segregation that occurred during cooling of the casting. The step cool heat treatment is quite different. The high temperature heat treatments release sulfur that was trapped at carbide interfaces, and possibly in sulfides. During step cooling, sulfur strongly segregated to the grain boundaries. A question remains as to why the step-cooled specimen had such a large sulfur concentration at the grain boundary relative to the exposed carbide surface. The eutectic, in this case probably Laves phase, did show an excess sulfur concentration equal to the grain boundary. This is somewhat reassuring since the driving force for segregation to grain boundaries, carbide-matrix and Laves-matrix interfaces should all be of a similar magnitude.

Distribution of Elements in Recrystallized Alloy Heats

Grain Boundaries

A series of 718-type heats were produced with controlled levels

of certain elements including P, S and B. These heats were thermomechanically treated to recrystallize the as-cast structure. This produced a significant increase in the probability of obtaining intergranular fracture in the Auger system.

The surface excesses of S, P and B are tabulated as histograms in Figures 12-15. It is apparent that when one of these elements is present in sufficient quantity, it finds its way to the grain boundaries. Due to space limitations, only representative data was tabulated. Variations were observed from boundary to boundary in the same sample. These variations were sometimes significant. The exception of this rule was S in the presence of carbides. Heats #5 and # 10 showed no grain boundary sulfur although it appeared in the alloy at a significant level. This is initially surprising considering the fabled surface activity of sulfur. Another interesting feature is that the presence of one element in significant concentration prohibits the segregation of other elements when they are present at a reduced level.

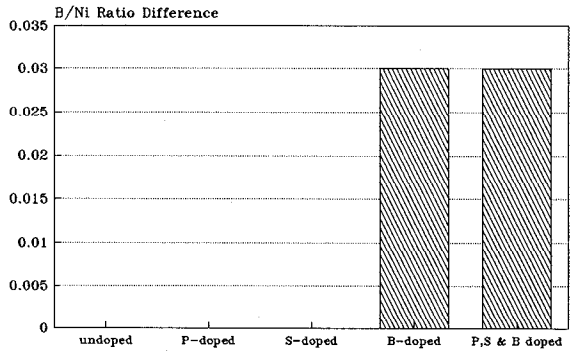

Figure 12 - Excess grain boundary boron for Alloys 20B, 14B, 13B, 3B and 22A.

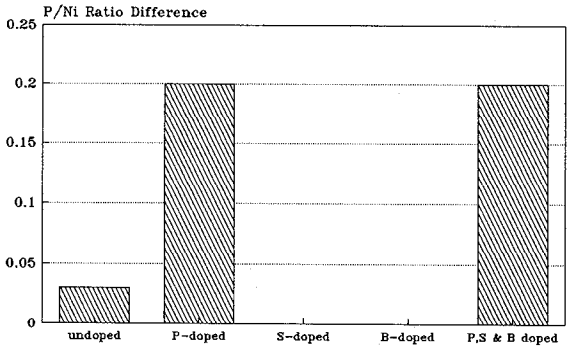

Figure 13 - Excess grain boundary phosphorus for Alloys 20B, 14B, 13B, 3B and 22A.

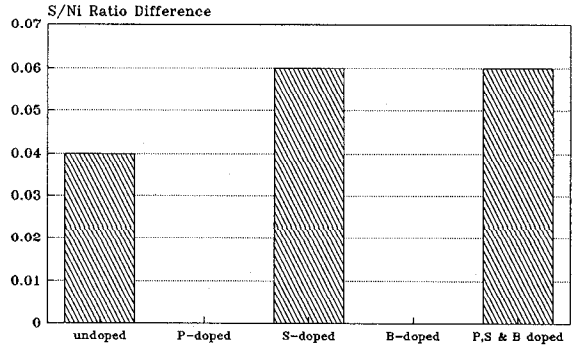

Figure 14 - Excess grain boundary sulfur for Alloys 20B, 14B, 13B, 3B and 22A.

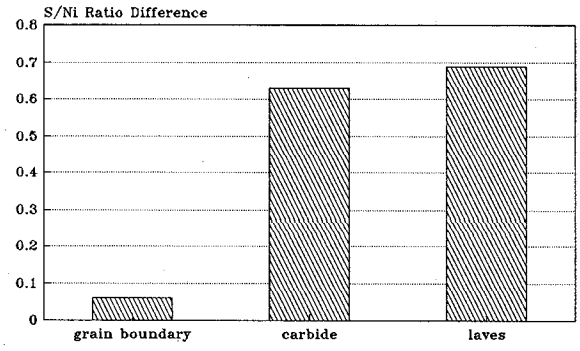

Figure 15 - Excess interface sulfur in Alloy 22A.

Carbides

The carbide-matrix interface in the recrystallized heats show the same behavior observed in the as-cast heats. Sulfur is found to segregate strongly at the carbide-matrix interface. This apparently occurred at the expense of sulfur segregation to the grain boundaries. Heats #10 and #5 both contain significant S concentration and exhibit strong carbide-matrix segregation but no grain boundary segregation of S. This apparently allows B, in the case of heat #10, to occupy grain boundary sites.

Conclusions

1. Sulfur segregates strongly to carbide and eutectic interfaces during solidification.

2. Sulfur reduces the strength of the carbide-matrix interface and makes it a preferred fracture path.

3. Sulfur redistributes to grain boundaries during step cool heat treatments such as a continuous solution anneal plus age hardening. A similar situation would exist during slow cooling of large castings.

4. Sulfur, phosphorous and boron all will segregate to grain boundaries when present in significant quantity. Their presence on the boundary can be inhibited by reducing their bulk concentration and by competition for grain boundary sites by other segregating elements.

5. Phosphorous is found on grain boundaries more so than at carbide-matrix interfaces and may indicate better solubility in the matrix than sulfur.

6. Boron is not strongly attracted to grain boundaries when present at relatively low concentrations.

Acknowledgment

The authors wish to thank NASA/MSFC for their support of this work and G.E. Gas Turbine Division for supplying materials.

References

1. C. G. Bieber and R. F. Decker: Trans. TMS-AIME, 1961, vol. 221, p. 629.

2. R. J. Henricks and M. L. Gell: "Trace Element Effects in Cast Nickel-Base Superalloys," ASM Materials Engineering Congress, Chicago, IL, 1973.

3. R. T. Holt and W. Wallace: Impurities and Trace Elements in Nickel-Base Superalloys," International Metals Review, 1976.

4. H. R. Gray: NASA TN D-7805, Jan. 1975.

5. J. M. Walsh and N. P. Anderson: Superalloys, Proc. of the Seven Springs Conference, AIME/TMS, Warrendale, PA, 1976, pp. 127-36.

6. C. L. White, J. H. Schneibel, and R. A. Padgett: Met. Trans A, vol. 14A, pp. 595-610.

7. B. J. Berkowitz and R. D. Kane: Corrosion, 1980, vol. 36, p. 24.

8. R. D. Kane and B. J. Berkowitz: Corrosion, 1980, vol. 36, p. 29.

9. A. W. Funkenbusch, L. A. Heldt, and D. F. Stein: Met. Trans A, vol. 13A, pp. 611-618.

10. E. E. Brown and D. R. Muzyka: Superalloys II, C. T. Sims, N. S. Stoloff, and W. C. Hagel, eds., John Wiley & Sons, New York, NY, 1987, pp. 165-183.

11. J. M. Walsh and B. H. Kear: Met. Trans A, 1975, vol. 6, pp. 226.

12. J. W. Schultz, Ph.D. thesis, University of Michigan, 1965, (University Microfilms Inc., Ann Arbor, Michigan, No. 65-11030).

13. R. A. Mulford, Metall. Trans. A, 1983, vol. 14A, pp. 865-70.

14. M. Guttmann and D. McLean, Interfacial Segregation, W. C. Johnson and J. M. Blakely, eds., ASM, Metals Park, Ohio, 1979, pp. 261-350.

APPENDIX A

Scanning Auger Microprobe Ratios of Peak Heights (Elements to Nickel)
for As-Cast and Heat Treated Specimens

Heat and Area of Surface

Peak Height Ratios*

Ni_{848}	Fe_{652}	Cr_{529}	O_{507}	Ti_{419}	N_{381}	C_{273}	Mo_{222}	B_{179}	Nb_{168}	S_{150}	P_{119}
Heat #20A											
GB											
1.00	.31	.67	.09	.04	.06	.08	.06	.00	.09	.02	.04
GB**											
1.00	.28	.66	.03	.09	.30	.17	.05	.00	.27	.00	.06
Laves											
1.00	.32	.70	.37	.24	.28	.11	.09	.00	.27	1.30	.04
Laves**											
1.00	.30	.63	.03	.13	.25	.04	.13	.00	.53	.00	.09
Ppt											
1.00	.38	.63	1.19	.19	.26	.20	.13	.00	.15	5.05	.00
MC											
1.00	.30	.62	.27	.42	.75	1.58	.07	.00	1.18	.00	.00
Matrix											
1.00	.27	.57	.09	.09	.10	.07	.04	.00	.15	.00	.03
Heat #25A											
GB											
1.00	.32	.68	.48	.07	.11	.11	.06	.00	.13	.02	.05
GB**											
1.00	.31	.60	.11	.07	.28	.00	.03	.00	.12	.02	.04
Laves											
1.00	.30	.61	.22	.14	.17	.17	.03	.00	.17	.19	.04
Ppt											
1.00	.30	.60	.58	.33	.66	.26	.00	.00	.19	2.09	.00
MC											
1.00	.32	.52	1.13	.63	.85	.82	.11	.00	.59	4.13	.13
MC**											
1.00	.36	.68	.24	.68	.91	.56	.00	.00	.95	2.41	.00
Matrix											
1.00	.33	.63	.25	.05	.07	.06	.03	.00	.04	.02	.01
Heat #22A											
GB											
1.00	.31	.68	.38	.06	.09	.04	.04	.00	.11	.03	.06
GB**											
1.00	.32	.60	.06	.08	.23	.00	.05	.00	.10	.00	.04
Ppt											
1.00	.30	.56	.40	.11	.16	.10	.07	.00	.24	1.01	.00
MC											
1.00	.32	.54	.97	.28	.48	1.02	.05	.00	.85	.00	.10
Matrix											
1.00	.28	.61	.17	.07	.09	.05	.03	.00	.13	.00	.03

Heat #27A

GB											
1.00	.33	.70	.36	.12	.14	.15	.08	.00	.20	.14	.07
GB**											
1.00	.33	.71	.05	.09	.25	.06	.08	.00	.28	.03	.07
Laves											
1.00	.30	.66	.03	.24	.39	.18	.05	.00	.40	.43	.07
MC											
1.00	.40	.63	1.08	2.07	2.64	3.42	.12	.00	1.88	4.61	.26
Matrix											
1.00	.28	.60	.16	.07	.06	.03	.04	.00	.11	.26	.03
Matrix**											
1.00	.24	.58	.00	.18	.36	.17	.04	.00	.19	.32	.06

Heat #27A following a homogenizing treatment of 1 hour at 1093C

GB											
1.00	.25	.59	.14	.06	.05	.10	.02	.00	.05	.09	.03
GB**											
1.00	.31	.71	.06	.09	.13	.07	.06	.00	.24	.06	.05
Laves											
1.00	.32	.57	.89	.14	.18	.27	.07	.00	.24	.75	.00
Ppt											
1.00	.39	.44	1.48	.20	.23	.49	.00	.11	.29	3.18	.00
MC											
1.00	.29	.59	.57	.58	.80	1.34	.07	.00	.97	1.81	.11
MC**											
1.00	.32	.62	.58	.41	.57	1.72	.10	.00	1.33	.00	.17
Matrix											
1.00	.34	.84	.23	.10	.14	.08	.10	.00	.22	.04	.06

Heat #27A following solution annealing of 1 hour at 927C

GB											
1.00	.32	.62	.10	.04	.05	.08	.03	.00	.04	.00	.02
Laves											
1.00	.32	.72	.17	.10	.15	.13	.04	.00	.15	.15	.02
Ppt											
1.00	.22	.56	.67	.78	.99	.97	.06	.00	.75	4.78	.04
MC											
1.00	.32	.65	.59	.29	.42	1.50	.08	.00	1.12	.00	.13
Matrix											
1.00	.31	.62	.09	.05	.06	.06	.03	.00	.05	.01	.01

Heat #27 following step-cooling treatment of 22 hours

GB											
1.00	.24	.49	.19	.41	.51	.14	.03	.00	.12	2.26	.05
GB**											
1.00	.30	.74	.08	.12	.26	.05	.09	.00	.21	.09	.05
Laves											
1.00	.28	.46	.68	.32	.50	.36	.07	.00	.28	2.02	.08
MC											
1.00	.36	.54	1.48	.69	1.15	3.02	.14	.00	2.34	.15	.36
Matrix											
1.00	.33	.60	.64	.12	.09	.08	.04	.00	.07	.06	.06

APPENDIX A (continued)

Peak Height Ratios*

Specimen/ Area	P^*_{119}	S_{150}	Nb_{168}	B^*_{179}	Mo_{222}	C_{273}	N^*_{381}	Ti_{419}	O_{507}	Cr_{529}	Ni_{848}
#3B											
g.b.	.23	.06	.16	.03	.08	.19	.15	.07	.16	.62	1.00
matrix	.00	.02	.13	.00	.03	.17	.12	.07	.21	.48	1.00
#5B											
g.b.	.22	.00	.14	.00	.06	.15	.09	.06	.10	.57	1.00
g.b. **	.00	.00	.09	.00	.06	.15	.26	.07	.13	.55	1.00
matrix	.00	.00	.04	.00	.00	.12	.12	.06	.28	.54	1.00
carbide	.00	1.90	1.17	.00	.08	2.29	.86	.64	.91	.62	1.00
carbide **	.00	.18	.85	.00	.07	1.10	.67	.39	.60	.50	1.00
carbide +	.00	.00	.83	.00	.11	1.05	.64	.35	.24	.50	1.00
#10B											
g.b. #1	.00	.04	.12	.02	.05	.18	.15	.05	.09	.53	1.00
g.b. #2	.00	.11	.13	.02	.06	.24	.16	.06	.06	.58	1.00
matrix	.00	.05	.08	.00	.03	.11	.09	.08	.24	.67	1.00
carbide	.31	.63	1.69	.00	.17	2.92	1.08	.82	1.77	.55	1.00
#12B											
g.b. #1	.00	.00	.20	.04	.05	.11	.07	.06	.15	.59	1.00
g.b. #2	.00	.00	.16	.03	.05	.09	.06	.06	.06	.59	1.00
matrix	.00	.00	.11	.00	.05	.10	.11	.09	.16	.62	1.00
#13B											
g.b.	.00	.03	.12	.03	.05	.06	.06	.06	.09	.64	1.00
matrix	.00	.03	.12	.00	.04	.10	.08	.07	.03	.59	1.00
#20B											
g.b. #1	.06	.04	.13	.00*	.08	.24	.09	.07	.48	.68	1.00
g.b. #1 **	.06	.00	.10	.00*	.04	.07	.30	.10	.13	.63	1.00
g.b. #2	.00	.00	.10	.00*	.03	.09	.06	.06	.19	.59	1.00
matrix	.00	.00	.10	.00*	.04	.12	.09	.09	.26	.64	1.00
precipitates	.00	.76	.08	.00*	.02	.12	.23	.15	.94	.45	1.00
#22A											
g.b. #2	.00	.02	.13	.00	.04	.07	.11	.07	.41	.68	1.00
g.b. #2 **	.00	.00	.15	.00	.07	.00	.21	.07	.05	.57	1.00
matrix	.00	.00	.12	.00	.02	.09	.10	.09	.12	.62	1.00
carbide	.00	.00	3.86	.00	.00	5.42	1.49	.98	.45	.62	1.00
eutectic	.00	1.01	.24	.00	.07	.10	.16	.11	.40	.56	1.00
#25A											
g.b. #1	.00	.01	.11	.00*	.06	.06	.07	.06	.23	.63	1.00
g.b. #1 **	.00	.02	.12	.00*	.03	.00	.28	.07	.11	.60	1.00
matrix	.00	.02	.04	.00*	.03	.06	.07	.05	.25	.63	1.00
carbonitride	.00	4.00	.68	.00*	.10	1.24	1.32	.85	.88	.46	1.00
eutectic	.00	.14	.16	.00*	.05	.13	.16	.14	.30	.57	1.00
#27A											
g.b.	.00	.14	.20	.00	.08	.15	.14	.12	.36	.70	1.00
g.b. **	.00	.00	.28	.00	.08	.06	.25	.09	.05	.71	1.00
matrix	.00	.00	.15	.00	.05	.06	.14	.09	.20	.56	1.00
carbide	.00	4.61	1.88	.00	.12	3.42	2.64	2.07	1.08	.63	1.00
#27A											
g.b.	.00	.09	.05	.00	.20	.10	.05	.06	.14	.59	1.00
matrix	.00	.00	.22	.00	.10	.08	.14	.10	.23	.84	1.00
carbide	.00	.00	1.33	.00	.10	1.72	.57	.41	.58	.62	1.00

eutectic	.00	2.12	.81	.00	.09	.80	.77	.60	.41	.48	1.00
carbide/ interface	.00	1.81	.97	.00	.07	1.34	.80	.58	.57	.59	1.00

* element peak height relative to Ni peak height (element/Ni)
** sputtered
\+ resputtered

* Because P overlaps with a small Nb peak, it must have a ratio of about 1:1 with Nb to be significant
* B overlaps with chlorine spectra
* N overlaps with Ti spectra